P2-66

Beryllium film deposition in cavity samples in remote areas of the JET divertor during the 2011-2012 ITER-like wall campaign

S. Krat[1,2], M. Mayer[2], U. von Toussaint[2], P. Coad[3], A. Widdowson[3], Yu. Gasparyan[1], A. Pisarev[1], and JET contributors[+]

EUROfusion Consortium, JET, Culham Science Centre, Abingdon, OX14 3DB, UK

[1]National Research Nuclear University "MEPhI", Moscow Kashirskoe sh. 31, 115409, Russia

[2]Max-Planck-Institut für Plasmaphysik, Boltzmannstr. 2, 85748 Garching, Germany

[3]Culham Science Centre, EURATOM/UKAEA – Fusion Association, Abingdon, Oxfordshire OX14 3DB, UK

[+] See the Appendix of F. Romanelli et al., Proceedings of the 25th IAEA Fusion Energy Conference 2014, Saint Petersburg, Russia

Abstract

Beryllium film deposition was studied with cavity samples in remote areas of the inner and outer JET divertor and below divertor tile 5 during the 2011-2012 campaign with the ITER-like wall. Predominantly beryllium films were formed inside the cavities with some additional carbon, the ratio Be/C was >2. These deposited layers had high D/(Be+C) ratios of about 0.3. The formation of these films is mainly due to sticking of beryllium-containing particles with low sticking coefficients < 0.5. The observed surface loss probabilities depend on the position in the divertor. The particles responsible for film deposition originated from areas in the divertor strike points.

PSI-22 keywords: Deuterium, Beryllium, co-deposition, JET

Corresponding Author Address: 115409, Russia, Moscow, Kashirskoe shosse 31

Corresponding Author e-mail: stepan.krat@gmail.com

Presenting Author: Stepan Krat

Presenting Author e-mail: stepan.krat@gmail.com

1. Introduction

Hydrogen isotopes, including radioactive tritium, can accumulate in fusion devices due to redeposition of materials eroded from plasma-facing components. This makes the study of material redeposition in remote shadowed areas an important topic from the viewpoint of fusion devices lifetimes and radiation safety.

It was already demonstrated that during operation with carbon walls thick hydrocarbon co-deposited layers containing large amounts of deuterium accumulated in remote areas of the JET divertor [1,2]. This accumulation was attributed mainly to transport of hydrocarbon radicals and small clusters from divertor tiles due to thermal decomposition and thermally activated chemical erosion during ELMs [3].

In 2010 the first wall of JET was changed from full carbon to the ITER-like wall (ILW) configuration consisting of beryllium in the main chamber and tungsten in the divertor [4]. A first experimental campaign with the ILW ran from 2011 to 2012 [5]. A number of results have already been reported [6] – a decrease in plasma impurities [7,8], change in main chamber wall erosion [9,10], and a change of the distribution and amount of deposits in the divertor [11–13]. Using several diagnostics, such as quartz microbalances and rotating collectors, deposition in the shadowed areas of the inner and outer divertor was investigated [11,14,15]. Significantly less deposition was observed on divertor tiles [12] and in the remote divertor regions [11,14,15]. This was attributed to a difference in Be and C erosion characteristics, as Be, unlike C, is not eroded by low ($E<10$ eV) and thermal energy D ions [6]. Because Be should not be transported into remote areas in the same way as hydrocarbons in JET-C campaigns, it is important to study the properties of the deposited layers there, and to determine the mechanism by which Be containing particles are transported into remote areas of the divertor.

In this paper, an analysis of beryllium film sources and surface loss probabilities in remote areas of the divertor of JET during the 2011-2012 campaign is presented and compared with the data for hydrocarbon films during JET-C campaigns [1].

2. Experimental

2.1. Cavity samples

Similarly to previous JET-C campaigns, cavity samples [16]were used to study film deposition in the shadowed areas of the divertor [1] . Cavity samples consist of two parallel Si plates, one atop another, with the top plate having a narrow (0.8 mm) entry slit through which particles can enter the cavity. There, they can stick to the bottom plate upon first impact with it, turn into a stable molecule, or be reflected from the bottom surface, and either impact the top plate, or leave the cavity through the entry slit. This process continues until the particles either are stuck to the surface, or leave the cavity.

The thickness distribution of the resulting deposited layers carries information about the sticking coefficient of the particles forming them, and about the directional distribution of entering particles. The sticking coefficient can be obtained by measuring the ratio of the total amount of particle on the top plate to the total amount of particles on the bottom plate – this value is mostly independent on the entering particles flux distribution, and can be used to initially estimate the sticking coefficient of the particles in the cavity.

In turn, if one knows the sticking coefficient of the film inside the cavity, it is possible to use the cavity as a pinhole camera and reconstruct the source distribution of the particles forming the film by matching experimental and numerically modeled film profiles. Profile matching can also be used for a more precise sticking coefficient estimation.

Three cavities were placed in the divertor of JET during the 2011-2012 campaign (fig. 1). They were located at the same places as those used during the 2005-2009 JET-C campaign: one close to the louvers of the inner divertor, one close to the louvers of the outer divertor and one under the tile 5 of the divertor. During this time 2819 successful discharges with 4.51×10^4 s total divertor plasma time were performed.

The cavity slits were oriented horizontal in toroidal direction facing the divertor plasma (see Fig. 1).

2.2.Ion beam analysis

Deposited layers were quantitatively analyzed using nuclear reaction analysis (NRA) using 2400 keV $^3He^+$ ions with a lateral resolution of 0.5 mm. Deuterium was detected using the $D(^3He,p)^4He$ [17] nuclear reaction. The $^{12}C(^3He,p)^{14}N$ reaction was used to detected carbon, and the $^9Be(^3He,p)^{11}B$ [18] reaction was used for Be. The NRA detector was covered with 5 μm Ni and 12 μm Mylar foils to stop backscattered ^3He ions. The spectra were analyzed using the SIMNRA program [19].

2.3.Computer simulation

Deposition inside the cavities was modeled using a Monte-Carlo simulation [20]. A 2-dimensional model was used, simulating the profile in the central plane of the cavity perpendicular to the entry slit.

At each surface the particles could stick with probability s or reflect with probability r. Particles are reflected with the cosine distribution from all surfaces in accordance with the experimental data [16]. s and r were constant for each given particle at all collisions.

The neutral gas pressure in the divertor is typically below 10^{-1} Pa [21]. A similar pressure range is assumed to be present inside the cavity samples. At this pressure the mean free path length is >8 mm so collisions with gas molecules inside the cavity can be neglected.

The incident particle flux was separated into 20 sub-fluxes, each consisting of particles entering the cavity with a random angle of incidence in a small range. The sum of all sub-flux ranges comprised the whole range of possible particle entry directions (angles of incidence <50°). The resulting particle flux was a linear combination of all sub-fluxes. Each sub-flux was modeled with a total of 4×10^{7} particles.

A database of profiles generated by individual sub-fluxes of particles with sticking coefficient s from 0.01 to 1 with a 0.01 step was generated. It was assumed that there were two groups of incoming particles with the same incoming particle flux distribution but with different sticking coefficients The deposited profiles were modeled with either one or two groups of incoming particles. To prevent highly irregular flux configurations it was assumed that neighboring sub-fluxes varied less than 50% from each other.

Additionally, profiles with a homogenous sub-flux intensity distribution and one sticking coefficient were used to obtain ratios of the total amount of particles on the bottom plate of the cavity to the total amount of particles on the top plate of the cavity. This ratio was then matched to the experimentally observed one to check the results obtained by profile-matching.

3. Results

3.1. Inner divertor

Experimental and modeled thickness profiles for Be, C and D inside the inner divertor cavity are shown in fig 2.

With JET-ILW there is far less deposition than was observed during JET-C campaigns. Normalizing to the campaign lengths, Be was deposited 30 times less than C was deposited during the 2005-2009 campaign, and 16 times less than C during the 1999-2001 campaign. Deuterium accumulation was 45 times less than during the 2005-2009 campaign and 33 times less than during the 1999-2001 campaign.

The films consisted of Be, C and D. Be was the predominant element, with an average C/Be=0.5. A high deuterium content with an average D/(C+Be)=0.26 was observed. The D content is highest near the entrance slit, D/(C+Be)=0.4 in a 4 mm wide stripe on the bottom plate. Such high D contents has been previously observed in D-Be codeposits [22].

Data for Be, D and C sticking coefficients obtained using a two species model, a one species model and ratios of total amounts of particles on top and bottom plates is shown in table 1. The two species model is not very precise, but the presence of a high-sticking species was consistently observed for Be and D, but not for C.

Be, D and C incoming particle flux distributions are shown in fig. 3. For Be it is similar to the one observed for hydrocarbon particles in JET-C campaigns. The maximum amount of particles originates from the sloped central area of divertor tile 4 near the strike points. The C particle source has a high amount of particles originating from the backside of tile 3. The deuterium particle source is a mixture between the sources of Be and C.

3.2.Tile 5 cavity

Experimental and modeled thickness profiles for Be, C and D inside the tile 5 divertor cavity are shown in fig 4.

The amounts of Be and D in the tile 5 cavity were almost the same as in the inner divertor cavity. The amount of carbon was times 25% smaller. The deuterium content in the film was on average D/(Be+C)=0.3. A lower relative carbon fraction than in the inner divertor, with an average C/Be=0.3 was observed.

Data for Be, D and C sticking coefficients obtained using the two species model, the one species model and ratios of total amounts of particles on top and bottom plates are shown in table 2.

Particle sources of all the elements forming the layers also show similarity to each other (fig. 5) Most of the particles entered the cavity from the direction of tile 3, and, specifically, from near the area of the lower strike point on tile 3. This is similar to the films observed in the septum cavity during the 1999-2001 experimental JET-C campaign [1].

3.3.Outer divertor cavity

Experimental and modeled thickness profiles for Be, C and D inside the outer divertor cavity are shown in fig 6.

The outer divertor cavity contained the largest amount of deposits: 3.7 times more Be, 1.4 times more C and 2.2 times more D than the inner divertor cavity. This corresponds well with the distribution of deposited materials on the inner and outer divertor plates [12].

The outer divertor cavity had the lowest C content, with an average C/Be=0.23. The average deuterium content was the same as in the other cavities.

Data for Be, D and C sticking coefficients obtained using the two species model, the one species model and ratios of total amounts of particles on top and bottom plates are shown in table 3.

The distribution of incident particles (fig 7) bears similarities to the one for the inner divertor cavity (fig 3). Most of D, Be and C originate from the direction near the center of divertor tile 6. Unlike for the inner divertor cavity, however, no significant carbon flux from the backside of tile 7 was observed.

4. Discussion

Compared to hydrocarbon films from JET-C campaigns [1], it is clear that a larger fraction of Be and D particles are retained on the inner side of the upper cavity plate. Two main reasons for this can be easily envisioned: high reflection probability from the surface, and/or re-erosion of deposited films by incident particles.

According to TRIM [23] calculations, there is no appreciable reflection of Be+ from Be for energies below 6 keV, and the maximum reflection of Be from Si occurs around 90 eV with a reflection coefficient of ≈0.15. According to [24] the Be self-reflection coefficient is below 0.12 at 100 eV.

The Be self-sputtering yield can be as high as 0.3-0.5 [25] depending on the angle of incidence. Be sputtering by D can have sputtering yields of about 0.1, especially at low surface temperatures, when chemically-enhanced sputtering can increase it at least by 1/3

[26]. As such, it is possible to sputter a large amount of Be from the area directly below the entry slit by energetic impinging particles.

If re-erosion would be the primary source of the high amount of particles on the top plate, then one would expect two key differences between modeled and experimental data. There would be a lot of particles concentrated on the top plate near the entry slit, and there would be very little to no particles on the bottom plate away from the cavity's entrance line of sight area (zone about 6 mm wide directly below the entrance slit). This is because unlike in the case of low sticking coefficients, particles re-eroded from the bottom plate would be redeposited on the top plate and remain there.

Such anomalously large amounts of Be on the top plate near the entry slit were observed for the outer divertor and the tile 5 cavities. However, significant amount of Be, at least about 10% of all Be in the cavities was observed on the bottom plate outside direct line of sight from the cavity entrance. Films were well modeled by using a constant sticking probability model, indicating that while re-erosion likely played a role in accumulation of particles on the top plate near the entry slit, it wasn't responsible for particle transport into remote areas. In the inner divertor cavity, no abnormal amounts of Be on the top plate near the entry slit were observed, indicating that re-erosion plays a lesser role for that area.

There was a difference between the layers in the inner divertor cavity and layers in the tile 5 and outer divertor cavities. No high sticking ($s>0.7$) species were observed outside of the inner divertor cavity. Film compositions were mostly uniform in the tile 5 and outer divertor cavities, with particle sources and sticking coefficients similar for Be, C and D containing particles. This means that for the inner divertor cavity an additional type of Be and D containing particles with high sticking coefficient is present. In [27] it was noted that, unlike the area under tile 5, the location of the inner divertor cavity was accessible for ions. It

might be that the high-sticking species observed in the inner divertor are the result of the ion flux into the cavity.

A large fraction of the C observed in the inner divertor cavity came from the direction of the backside of tile 3. Even in full metal machines such as ASDEX Upgrade or JET deposition of carbon is always observed on divertor tiles. The origin of this carbon was never unambiguously identified and it was already speculated that carbon may originate by arcing or by erosion of uncoated carbon tile side faces and rear sides [28]. The current observation of carbon originating from the rear side of tile 3 is the first direct observation of a carbon source at the uncoated rear side of a tile. Parasitic discharges [29] or chemical erosion by thermal atomic deuterium can be the source of these particles. D is co-deposited with both Be and C in the inner divertor cavity. This can be seen by its incoming particle flux distribution which is a mixture between that for Be and C, with a relatively large amount of particles coming from the backside of tile 3, and by the presence of high-sticking D species that could only be co-deposited with Be.

The precise mechanism explaining the observed low sticking probability of particles entering the cavity cannot be explained in detail at the moment. Chemical interaction between Be and D is one possible explanation.

The large C/Be ratio hints to a difference in Be and C transport, as explained in [11]. C is transported in a step-wise erosion-redeposition cycle, in part due to chemical erosion by low or thermal energy particles, while for Be a clear barrier at 10 eV exists [6], resulting in C being transported disproportionately into remote areas.

5. Conclusions

Layer deposition in remote areas of the inner and outer JET divertor as well as under tile 5 was measured using cavity samples during the first ILW campaign 2011-2012. These deposited layers are mainly composed of Be, with some C (C/Be=0.2-0.5) impurities and a high D content (D/(Be+C)=0.3-0.4) comparable to that in hydrocarbon films. A factor of about 50 decrease in the D accumulation rate was observed, and a more than one order of magnitude lower Be deposition rate compared to the C deposition rate during JET-C campaigns.

The observed films are formed mainly by particles with low sticking coefficients (s≈0.3). Re-erosion is thought to play a role, especially in the outer divertor and tile 5 cavities, but cannot explain all the observed results. Models of Be-Be reflection based on pair collisions can't adequately explain the observed phenomenon either.

In the inner divertor particles with higher sticking coefficients (>0.7) were observed. The difference is attributed to the ion flux that can enter the inner divertor cavity, but not the tile 5 cavity, where no highly-sticking particles were observed.

Particles forming the films inside the cavitites originated mostly from the strike point on tile 4 for the inner divertor, the strike point on tile 3 for the cavity below tile 5, and the strike point on tile 6 for the outer divertor cavity sample. An additional source of carbon located on the lower backside of the tile 3 was also observed.

Acknowledgements

This work has been carried out within the framework of the EUROfusion Consortium and has received funding from the Euratom research and training programme 2014-2018 under grant

agreement No 633053. The views and opinions expressed herein do not necessarily reflect those of the European Commission

1. Krat S. et al. Hydrocarbon film deposition inside cavity samples in remote areas of the JET divertor during the 1999–2001 and 2005–2009 campaigns // J. Nucl. Mater. 2014.

2. Coad J.P.P. et al. Erosion/deposition issues at JET // J. Nucl. Mater. 2001. Vol. 290, № 0. P. 224–230.

3. Kreter A. et al. Nonlinear impact of edge localized modes on carbon erosion in the divertor of the JET tokamak // Phys. Rev. Lett. 2009. Vol. 102, № 4.

4. Matthews G.F. et al. JET ITER-like wall—overview and experimental programme // Phys. Scr. 2011. Vol. T145. P. 14001.

5. Romanelli F. Overview of the JET results with the ITER-like wall // Nucl. Fusion. 2013. Vol. 53, № 10. P. 104002.

6. Brezinsek S. et al. Beryllium migration in JET ITER-like wall plasmas // Nucl. Fusion. Institute of Physics Publishing, 2015. Vol. 55, № 6. P. 063021.

7. Matthews G.F. Plasma operation with an all metal first-wall: Comparison of an ITER-like wall with a carbon wall in JET // J. Nucl. Mater. 2013. Vol. 438, Suppl, № 0. P. S2–S10.

8. Brezinsek S. et al. Residual carbon content in the initial ITER-Like Wall experiments at JET // J. Nucl. Mater. 2013. Vol. 438, № SUPPL. P. S303–S308.

9. Brezinsek S. Plasma-surface interaction in the Be/W environment: Conclusions drawn from the JET-ILW for ITER // J. Nucl. Mater. 2015. Vol. 463. P. 11–21.

10. Krat S. et al. Erosion at the inner wall of JET during the discharge campaign 2011–2012 in comparison with previous campaigns // J. Nucl. Mater. Elsevier B.V., 2015. Vol. 456. P. 106–110.

11. Esser H.G. et al. Material deposition on inner divertor quartz-micro balances during ITER-like wall operation in JET // J. Nucl. Mater. Elsevier, 2015. Vol. 463. P. 796–799.

12. Mayer M. et al. Erosion and deposition in the JET divertor during the first ILW campaign // Phys. Scr. 2016. Vol. 2016, № T167. P. 14051.

13. Bykov I. et al. Studies of Be migration in the JET tokamak using AMS with 10Be marker // Nucl. Instruments Methods Phys. Res. Sect. B Beam Interact. with Mater. Atoms. 2016. Vol. 371. P. 370–375.

14. Beal J. et al. Deposition in the inner and outer corners of the JET divertor with carbon wall and metallic ITER-like wall // Phys. Scr. Institute of Physics Publishing, 2016. Vol. T167, № T167. P. 14052.

15. Beal J. et al. Analysis of rotating collectors from the private region of JET with carbon wall and metallic ITER-like wall // J. Nucl. Mater. 2015. Vol. 463. P. 818–821.

16. von Keudell A. et al. Surface loss probabilities of hydrocarbon radicals on amorphous hydrogenated carbon film surfaces: Consequences for the formation of re-deposited layers in fusion experiments // Nucl. Fusion. 1999. Vol. 39, № 10. P. 1451–1462.

17. Alimov V.K., Mayer M., Roth J. Differential cross-section of the D(3He,p)4He nuclear reaction and depth profiling of deuterium up to large depths // Nucl. Instruments Methods Phys. Res. Sect. B Beam Interact. with Mater. Atoms. 2005. Vol. 234, № 3. P. 169–175.

18. Wolicki E.A. et al. DIFFERENTIAL CROSS SECTIONS FOR THE BE-9(HE-3,P)B-11 REACTION // Phys. Rev. 1959. Vol. 116, № 6. P. 1585–1591.

19. Mayer M. SIMNRA User's Guide. Garching, Germany: Max-Planck-Institut für Plasmaphysik, Germany, 1997. № IPP 9/113.

20. Toussaint U. von. unpublished.

21. Philipps V. et al. Dynamic fuel retention and release under ITER like wall conditions in JET // J. Nucl. Mater. 2013. Vol. 438, № SUPPL. P. S1067–S1071.

22. De Temmerman G. et al. An empirical scaling for deuterium retention in co-deposited beryllium layers // Nucl. Fusion. 2008. Vol. 48, № 7. P. 075008.

23. Ziegler J.F. SRIM.org [Electronic resource].

24. IAEA. ALADDIN Database [Electronic resource]. URL: https://www-amdis.iaea.org/ALADDIN/.

25. Eckstein W. Sputtering yields // Sputtering by Particle Bombardment, Topics in Applied Physics / ed. Eckstein W. 2007. Vol. 110, № 110. P. 33–187.

26. Brezinsek S. et al. Study of physical and chemical assisted physical sputtering of beryllium in the JET ITER-like wall // Nucl. Fusion. Institute of Physics Publishing, 2014. Vol. 54, № 10. P. 103001.

27. Kirschner A. et al. Modelling of the material transport and layer formation in the divertor of JET: Comparison of ITER-like wall with full carbon wall conditions // J. Nucl. Mater. 2015. Vol. 463. P. 116–122.

28. Kallenbach A. et al. Non-boronized compared with boronized operation of ASDEX Upgrade with full-tungsten plasma facing components // Nucl. Fusion. 2009. Vol. 49, № 4. P. 045007.

29. Vizgalov I.V., Pisarev A.A., Gutorov K.M. A mechanism of PFM erosion and

redeposition in gaps // J. Nucl. Mater. 2007. Vol. 363-365. P. 966–971.

Figure captions

Table 1: Sticking coefficients of Be, D and C in the inner divertor cavity obtained using profile matching with a two and a one species model and from the ratios of total amounts of particles on the top and bottom plates of the cavities. Percentages for the two species model are indicated for incoming particle fluxes.

Table 2: Sticking coefficients of Be, D and C in the tile 5 cavity obtained using profile matching with a two and a one species model and from the ratios of total amounts of particles on the top and bottom plates of the cavities.

Table 3: Sticking coefficients of Be, D and C in the outer divertor cavity obtained using profile matching with a two and a one species models and from the ratios of total amounts of particles on the top and bottom plates of the cavities.

Figure 1: Positions of cavity samples in the JET divertor during the 2011-2012 campaign. Strike point distributions in the same campaign are shown at the bottom.

Figure 2: Deposition inside the inner divertor cavity during the 2011-2012 campaigns, experimental data (dots) and modeling (lines). The deposition on the bottom plate is shown in the lower part of the figure, the deposition on the inner top plates is shown in the upper part. Note that the axis for the top plates is from top to bottom

Figure 3: Reconstructed incident particle flux distributions for the inner divertor cavity sample during the 2011-2012 campaign. The lengths of the bins in the polar diagram show the relative amounts of particles (Be, C, D) coming into the cavity from the directions indicated. The strike point distribution on tile 4 is indicated along its surface.

Figure 4: Deposition inside the tile 5 cavity during the 2011-2012 campaign, experimental data (dots) and modeling (lines). See Fig. 2 for details

Figure 5: Reconstructed incident particle flux distributions for the divertor tile 5 cavity sample during the 2011-2012 campaign. The strike point distribution on tile 3 is indicated along its surface.

Figure 6: Deposition inside the outer divertor cavity during 2011-2012 campaign, experimental data (dots) and modeling (lines). See Fig. 3 for details

Figure 7 Reconstructed incident particle flux distribution for the outer divertor cavity sample during the 2011-2012 campaign. The strike point distribution on tile 6 is indicated along its surface.

Table 1

	Two species model	One species model	Ratio matching
Be	91%*0.33+9%*0.97	0.4	0.46
D	48%*0.49+52%*0.76	0.64	0.68
C	17%*0.01+82%*0.53	0.44	0.53

Table 2

	Two species model	One species model	Ratio matching
Be	100%*0.21	0.21	0.14
D	100%*0.28	0.28	0.13
C	100%*0.14	0.14	<0.01

Table 3

	Two species model	One species model	Ratio matching
Be	100%*0.33	0.31	0.14
D	100%*0.31	0.33	0.33
C	100%*0.27	0.27	0.28

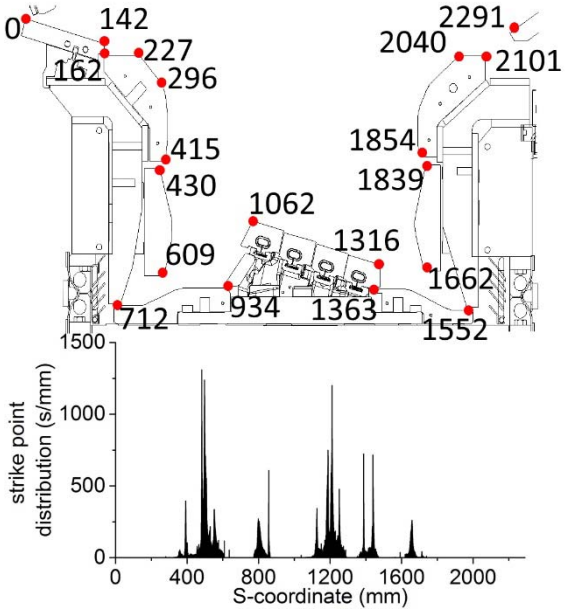
0
142
227
162
296
415
430
609
712
1062
934
1316
1363
2291
2040
2101
1854
1839
1662
1552
1500
1000
500
0
strike point
distribution (s/mm)
0
400
800
1200
1600
2000
S-coordinate (mm)

Figure 1

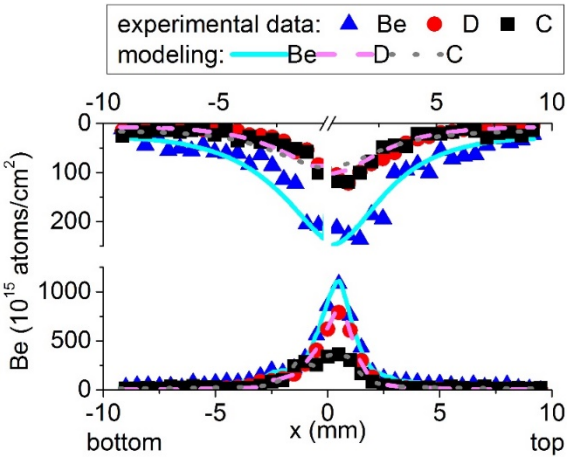
experimental data: Be D C
modeling: Be D C
-10
-5
5
10
0
100
200
1000
500
0
Be (10^15 atoms/cm^2)
-10
-5
0
5
10
x (mm)
bottom
top

Figure 2

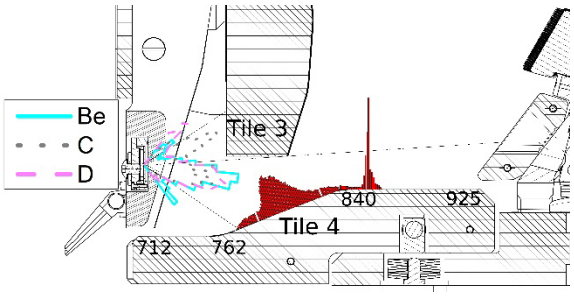

Figure 3

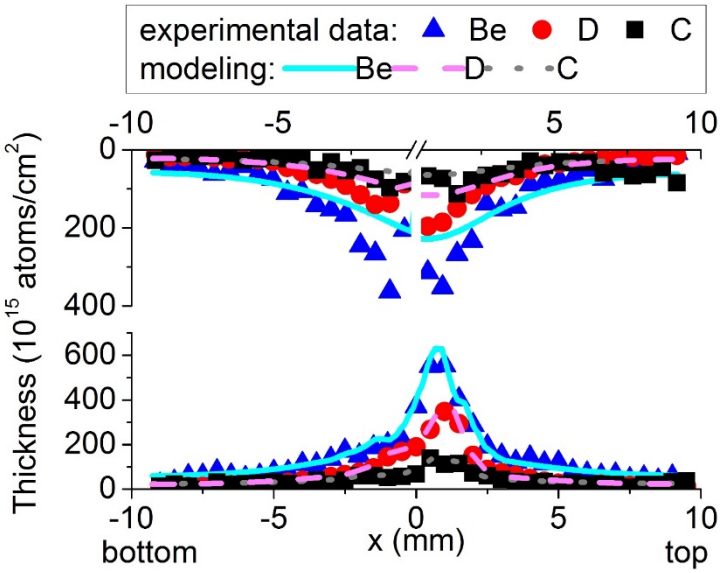
experimental data: Be D C
modeling: Be D C
Thickness (10^{15} atoms/cm^2)
x (mm)
bottom
top

Figure 4

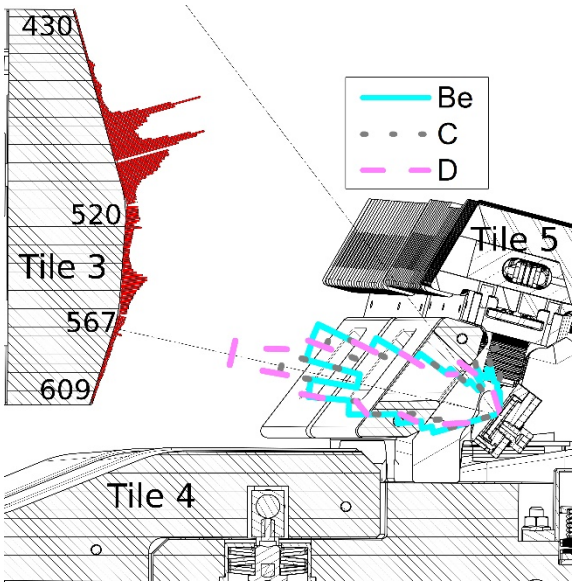

Figure 5

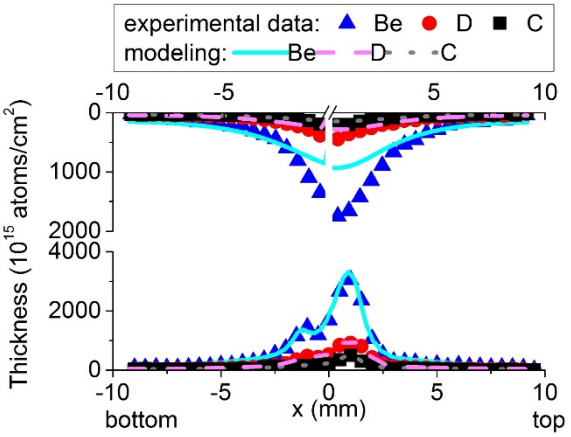
experimental data: Be D C
modeling: Be D C
Thickness (10^{15} atoms/cm^2)
0
1000
2000
4000
2000
0
-10
-5
5
10
-10
-5
0
5
10
x (mm)
bottom
top

Figure 6

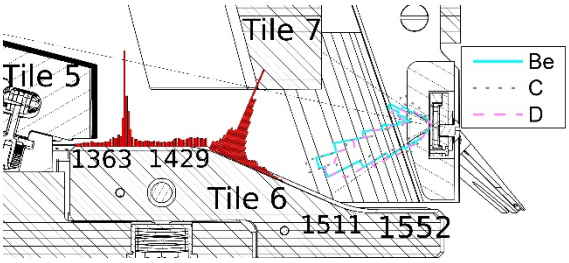

Fig. 7